Influence of Postdrawing Temperature on Mechanical Properties of Melt-Spun Isotactic Polypropylene

Tilo Schimanski,[†] Ton Peijs,[†,‡,§] Piet J. Lemstra,[†,‡] and Joachim Loos*[,†,‡]

Laboratory of Polymer Technology, Department of Chemical Engineering and Chemistry, and Dutch Polymer Institute, Eindhoven University of Technology, P.O. Box 513, 5600 MB Eindhoven, The Netherlands, and Department of Materials, Queen Mary University of London, Mile End Road, London E1 4NS, UK

Received July 7, 2003; Revised Manuscript Received November 13, 2003

ABSTRACT: Mechanical properties of melt-spun and postdrawn isotactic polypropylene (iPP) are studied to examine the dependence on the temperature in the postdrawing stage. In accordance with the literature, the Young's modulus is uniquely determined by the applied draw ratio. However, in contrast to the literature, we found that the overall mechanical behavior strongly depends on the applied postdrawing temperature. For a fixed draw ratio, a significant drop in yield stress can be observed with decreasing drawing temperature. At a certain drawing temperature, this drop leads to a transition from brittle to ductile failure behavior. From this study it can be concluded that a proper choice of drawing conditions offers control on several mechanical properties (e.g., stiffness, strength) at the same time.

Introduction

Polypropylene is apparently the major polymeric construction material of future in view of its impressive consumption in the past decade. However, polypropylene needs reinforcement to meet the high demands on stiffness and strength in engineering applications. Glass fibers are the major used reinforcing element. However, glass fibers cause environmental problems, in both mechanical and thermal recycling (incineration). Therefore, we are developing so-called "all-PP" composites, which are polypropylene matrices reinforced with high-stiffness, high-strength polypropylene tapes or fibers.[1,2] The mechanical properties of these composites are desired to be comparable with glass fiber reinforced polypropylene. To improve the tensile properties of the reinforcing PP component, a systematic study has been performed to optimize a tape-manufacturing route and to evaluate the influence of processing parameters.

Fundamental studies on melt spinning of isotactic polypropylene (iPP) date back to the 1960s, when the polymer of commercial significance just emerged.[3−5] The influence of spinning conditions on structure development and resulting mechanical properties for melt-spun filaments has been reported extensively in the literature.[6−11] Mainly the influence of extrusion temperature, take-up velocity, spin-line stress, and materials characteristics such as molecular mass and molecular mass distribution has been examined. Several studies describe the effect of additional cold drawing and annealing in the manufacturing process.[12−16] It is commonly concluded that mechanical properties like stiffness, strength, and elongation at break of cold drawn fibers/tapes uniquely depend on the applied draw ratio. The influence of drawing temperature is considered to be insignificant.[16]

This conclusion is in contrast to our results obtained by tensile tests performed on solid-state drawn iPP tapes and fibers. The measured Young's modulus is found to be independent of drawing temperature and uniquely determined by the applied draw ratio, in accordance with the Smith−Irvine model.[17,18] However, we found that the yield stress and the elongation at break are strongly influenced by the drawing temperature.

Density, retractive force, and wide-angle X-ray measurements have been performed to investigate the influence of postdrawing temperature and to correlate the resulting morphology with the mechanical properties.

Experimental Section

The isotactic polypropylene homopolymer (PLZ-937), used for tapes, was kindly supplied by Montell, Italy (now Basell, The Netherlands). The material has an average molecular mass of $M_w = 5 \times 10^5$ g/mol and a molecular mass distribution of $M_w/M_n = 5.6$.

Fibers were spun from a precommercial iPP fiber grade (X-7284) kindly supplied by DSM, The Netherlands. This material has an average molecular mass of $M_w = 2.8 \times 10^5$ g/mol and a molecular mass distribution of $M_w/M_n = 5.8$.

The tapes were prepared at Lankhorst/Indutech B.V. (The Netherlands) using a tape manufacturing line consisting of extruder, nozzle, water bath (18 °C), godet, oven, and winder.

The godet speed is referred to the speed at which the tape enters the oven. The winder speed determines the velocity at which the tape comes out of the oven. The postdraw ratio (λ) within the oven is determined by the ratio of winder speed and godet speed. The presented results are based on tapes that are postdrawn to the ratio $\lambda = 5$. The godet had a speed of 8 m/min, and the corresponding velocity of the winder was 40 m/min. While all processing parameters, especially the output of the extruder, were kept constant, the oven temperature was varied from 80 to 120 °C.

Fibers were prepared using a custom fabricated laboratory scale melt-spinning device. It consists of a double-walled storage cylinder combined with a capillary of 1.3 mm diameter and a length of 8 mm. The capacity of the storage cylinder is about 10 g of PP material. The material is pressed through the capillary by a piston driven by a hydraulic unit. The temperatures of storage cylinder and capillary are computer-controlled. At a processing temperature of 200 °C the filament from the capillary was winded on a drum at a rate of 10 m/min. The next step in fiber preparation was postdrawing of the filament in the solid state using a custom-built drawing unit.

[†] Department of Chemical Engineering and Chemistry, Eindhoven University of Technology.
[‡] Dutch Polymer Institute, Eindhoven University of Technology.
[§] Queen Mary University of London.
* Corresponding author. E-mail: j.loos@tue.nl.

10.1021/ma034949s CCC: $27.50
Published on Web 02/07/2004

The unit consists of two small drums of 48.5 mm diameter separated by a 600 mm long ceramic oven. Absolute speeds, velocity ratio of the two drums, and temperature are computer-controlled. The fibers were postdrawn at 60 and 120 °C with a postdraw ratio (velocity ratio of the two drums of the drawing unit) of $\lambda = 4$.

The mechanical properties of the postdrawn tapes were measured at room temperature using a Frank (Germany) tensile tester equipped with an extensometer, force reducing clamps, and a load cell of 500 N. The tensile tests were carried out with tapes of initial gauge length of 150 mm and at a crosshead speed of 150 mm/min. A set of 10 tensile tests was performed on each tape. Retractive force measurements were performed using the same Frank tensile tester, now equipped with an oven. The tapes were clamped with a fixed gauge length of 100 mm and a preload of 2 N. While heating the oven with a rate of about 5 °C/min the force on the clamps (as a response of the material) was recorded at intervals of 5 °C starting from 40 °C. Performing each retractive force experiment twice proved the reproducibility.

To relate the measured tensile force to the cross-section area, thickness and width of the drawn tapes were measured. The thickness was determined with a Twin-Check (Heinrich List GmbH, Germany) layer thickness measuring instrument using a magnetic−inductive method. The instrument has an accuracy of 1% of the measured value. The width was measured with a magnifying glass equipped with a scale bar. For both dimensions the average of 20 independent measurements spread over a tape length of 20 m was taken as a representative value.

Fibers were tested using a Zwick 1435 (Germany) tensile tester equipped with a load cell of 100 N and pneumatic fiber clamps. The tensile tests were carried out with fibers of initial gauge length of 100 mm and at a crosshead speed of 50 mm/min. A set of 10 tensile tests was performed on each fiber. The fiber diameter was measured with a light microscope equipped with a scale bar. The cross-section area of the fiber was calculated using the average value of 20 independent diameter measurements.

Wide-angle X-ray diffraction (WAXD) patterns of the tapes were recorded on a transmission pinhole camera with an exposure time of 3 h. A Philips PW-1120 X-ray generator working at 40 kV and 30 mA created the X-ray beam. The Cu Kα radiation had an average wavelength of 1.542 Å, while the Cu Kβ radiation was eliminated by a Ni filter.

Additional wide-angle X-ray measurements were performed using a monochromatic synchrotron beam of wavelength 0.718 Å available on beamline ID11-BL2 at the European Synchrotron Radiation Facility in Grenoble, France. Each diffraction pattern was recorded for 25 s on a two-dimensional CCD detector. Using the FIT2D program developed by Dr. Hammersly (ESRF), these 2-dimensional X-ray patterns were transformed into one-dimensional patterns by performing integration along the azimuthal angle.

The density of the drawn tapes was measured with a density column at room temperature. The column had a density gradient with start and end densities of 880 and 930 kg/m^3, respectively, and was prepared using distilled water and isopropyl alcohol according to the method described by Tung and Taylor.[19] The samples were allowed approximately 6 h to seek their level of displacement in the column. From the density the according mass crystallinity index X_c was calculated as a percentage using the following equation:[20,21]

$$X_c = \frac{\rho_c}{\rho}\left(\frac{\rho - \rho_a}{\rho_c - \rho_a}\right) \times 100\ (\%) \qquad (1)$$

where ρ represents the measured density of the tape, $\rho_c = 938$ kg/m^3 is the density of 100% crystallinity, and $\rho_a = 854$ kg/m^3 is the density of amorphous isotactic polypropylene.[22]

Results

A set of stress−elongation curves of postdrawn tapes ($\lambda = 5$) is shown in Figure 1. All tapes exhibit the same

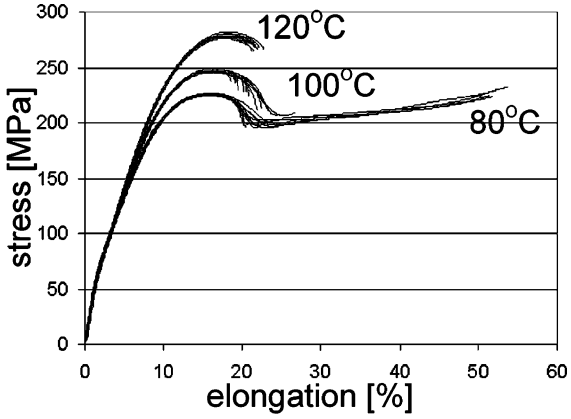

Figure 1. Stress−strain plots of iPP tapes, solid-state drawn ($\lambda = 5$) at different drawing temperatures as indicated in the diagram.

average stiffness of about 4.8 GPa, independent of the postdrawing temperature. The spread in ultimate elongation of the tapes drawn at 100 °C is significantly large; however, all stress−elongation curves have the same general characteristics; the different ultimate elongation can be assigned to local failures within the tapes. The constancy of the stiffness is in agreement with the Smith−Irvine model, which predicts that the Young's modulus uniquely depends on the applied network draw ratio λ_{net} according to the following equation:[17,18]

$$E = \left(E_u^{-1} - \left[\frac{3\lambda_{net}^3}{2(\lambda_{net}^3 - 1)}(1 - [\lambda_{net}^3 - 1]^{-1/2} \tan^{-1}[(\lambda_{net}^3 - 1)^{1/2}]) - \frac{1}{2}\right](E_u^{-1} - E_o^{-1})\right)^{-1} \qquad (2)$$

where E_o and E_u are the tensile moduli of perfectly oriented and nonoriented polypropylene, respectively. The network draw ratio λ_{net} is determined as the ratio to which an isotropic sample is drawn in an affine solid-state drawing process. With $E_o = 60$ GPa and $E_u = 0.6$ GPa, arrived as the best fit value, we obtain from eq 2 that a stiffness of 4.8 GPa corresponds to $\lambda_{net} = 7.1$. Therefore, the network draw ratio λ_{net} is higher than the applied postdraw ratio λ, which was equal to 5. The reason for this inconsistency is that the tapes are already preorientated before they are postdrawn in the oven. The preorientation results from the extrusion process and the consecutive drawing of the extrudate by the godet. Since the extruder setup and the godet speed were kept constant, we assume the preorientation to be a constant for all prepared tapes. The preorientation can be expressed by a corresponding λ_{pre}, which would generate the same orientation when applied on an isotropic sample.

Using

$$\lambda_{net} = \lambda_{pre}\lambda \qquad (3)$$

we obtain $\lambda_{pre} = 1.42$. Therefore, the tapes have a preorientation before drawing in the oven, which is equal to the orientation of an initially isotropic sample after drawing to 1.42 times.

While the drawing temperature does not influence the stiffness, a significant drop in yield stress can be observed by lowering the drawing temperature from 120 to 80 °C. Drawing at 120 °C results in tapes having a yield stress of about 280 MPa, whereas the yield stress

Table 1. Average Young's Modulus (E), Average Yield Stress (σ), and Standard Deviation of the Yield Stress ($\Delta\sigma$) of Solid-State Drawn ($\lambda = 5$) iPP Tapes in Dependence on the Applied Postdrawing Temperature (T_{draw})

T_{draw} [°C]	E [GPa]	σ [MPa]	$\Delta\sigma$ [MPa]
80	4.84	225.6	0.8
100	4.86	247.2	0.9
120	4.79	278.7	1.6

for tapes drawn at 80 °C is only on the order of 225 MPa. The decrease in yield stress is accompanied by a transition from brittle to ductile failure. The elongation at break of tapes drawn at 80 °C is obviously higher than of those drawn at 120 °C. The area beneath the stress−strain plots can be related with the impact resistance of the tapes; thus, tapes drawn at 80 °C offer higher energy absorption than the tapes drawn at 120 °C. An overview of average values for stiffness and yield stress is given in Table 1. The low standard deviations of the yield stress reflect the remarkable reproducibility of the measurements using tapes.

To prove whether this unexpected overall mechanical behavior is caused by inadequacies in the postdrawing process, the measured thickness and width of the postdrawn tapes were related to the theoretical values calculated for a purely uniaxial deformation under the assumption of constant volume. The theoretical thickness (d) for a certain postdraw ratio (λ) results from

$$d = \frac{d_0}{\sqrt{\lambda}} \tag{4}$$

where d_0 represents the thickness of the tape before postdrawing. The same formula can be used to calculate the theoretical width (w) by replacing d and d_0 by w and w_0, respectively. To generate theoretical curves for thickness/width vs postdraw ratio, which are independent from the dimensions of the precursor tape, the values for d and w were normalized by dividing by d_0 and w_0, respectively.

The authors are aware of the slight inaccuracy for theoretical thickness values obtained by the assumption of constant volume. More precise is the assumption of constant mass, which takes in account changes in density while postdrawing. For constant mass, eq 4 changes to

$$d = \frac{d_0}{\sqrt{\lambda x}} \tag{5}$$

where

$$x = \frac{\rho}{\rho_0} \tag{6}$$

is the ratio between density ρ of the postdrawn tape and density ρ_0 of the as-extruded tape.

However, measurements on a series of tapes postdrawn at a constant temperature (120 °C) with $\lambda = 2$ to $\lambda = 10$ have shown an increase in density by less than 2% compared to the as-extruded tape. Therefore, corrections for the theoretical thickness, obtained under the assumption of constant mass, are very small and were neglected. As can be seen from Figure 2, measured thickness and width of tapes produced on the above-

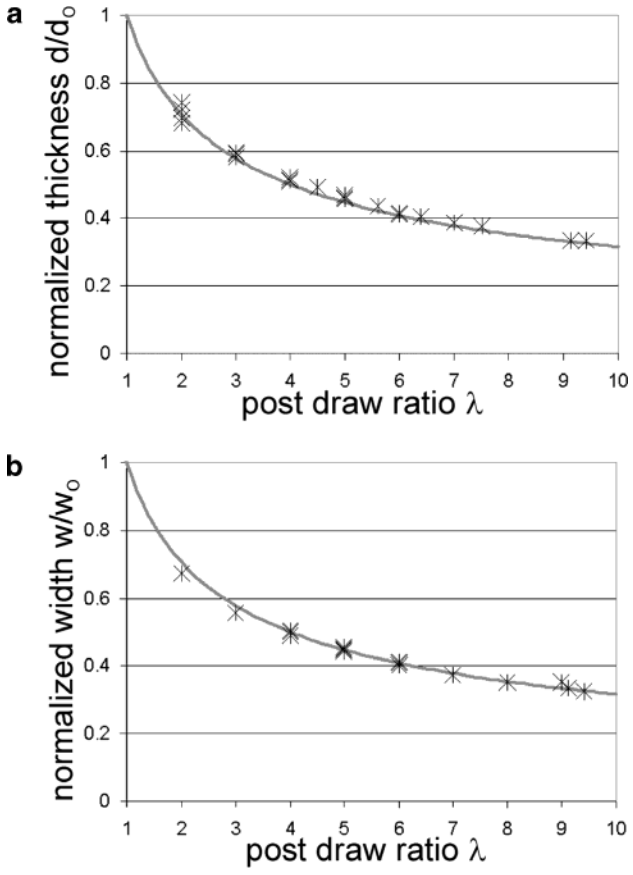

Figure 2. Normalized thickness/width of postdrawn tapes vs postdraw ratio (λ): (a) normalized thickness and (b) normalized width.

described manufacturing line fit very well to the theoretical curve and are independent of postdrawing temperature.

This implies that the prepared tapes are uniaxially deformed while drawing and that the postdraw ratio (λ) is uniquely determined by the ratio of winder speed and godet speed. Furthermore, the outer appearance indicates that the tapes are not affected adversely either at 80 or at 120 °C drawing temperature. All postdrawn tapes are transparent, reflecting that the tapes were not damaged by cavitations or voiding.

To prove that the observed influence of drawing temperature on yield stress and elongation at break is independent of the sample geometry, additional tensile tests were performed on postdrawn iPP fibers. In Figure 3 a set of stress−elongation curves of postdrawn fibers ($\lambda = 4$) is shown. Although the mechanical behavior of the fibers is not as homogeneous as the behavior of the tapes, the same significant drop in yield stress can be observed by lowering the postdrawing temperature.

Since the differences in overall mechanical behavior cannot be attributed to shortcomings within the postdrawing process or to the sample geometry, it is examined whether these differences are reflected by variations of the internal structures and morphologies of the samples. To investigate the influence of postdrawing temperature on crystallinity and on the organization of the crystalline and amorphous phases, X-ray, density, and retractive force experiments were performed.

Figure 4 shows wide-angle X-ray diffraction patterns of tapes drawn at 120 and 80 °C. For both tapes, the occurrence of sharp reflections is a clear indication for a fiber pattern. Tapes drawn at 120 °C possess a smaller

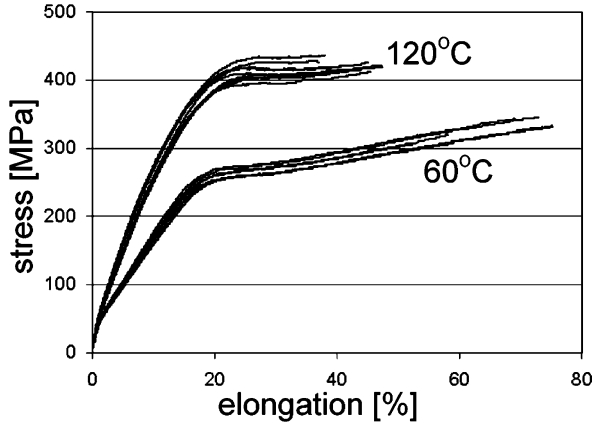

Figure 3. Stress−strain curves of iPP fibers, solid-state drawn ($\lambda = 4$) at different drawing temperatures as indicated in the diagram.

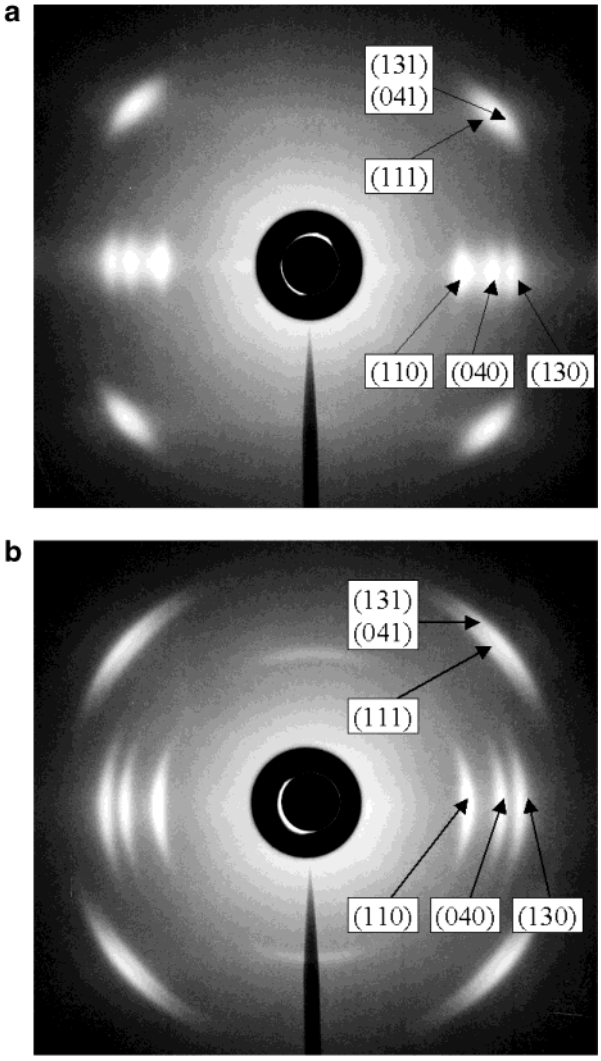

Figure 4. Wide-angle X-ray diffraction patterns of iPP tapes solid-state drawn at (a) $T_D = 80$ °C and (b) $T_D = 120$ °C.

radial peak width compared to those drawn at 80 °C. This can be clearly seen from the (111) and [(131)(041)] peaks in the diffraction patterns. At the drawing temperature of 120 °C one can distinguish between these peaks, while they are blurred in the pattern at drawing temperature of 80 °C. The smaller radial peak width reflects a larger crystal size and/or higher crystal perfection in the case of the higher drawing temperature.

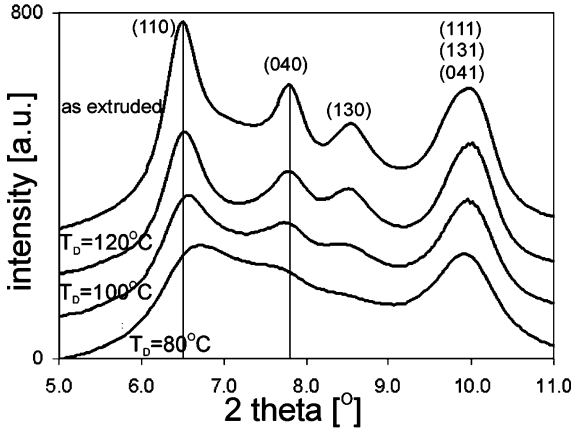

Figure 5. One-dimensional intensity scans integrated along the azimuthal angle of the two-dimensional X-ray pattern, drawing temperatures as indicated in the diagram.

From the patterns one can also observe that the peaks have different arc lengths depending on the drawing temperature. The arc length can be associated with the broadness of the orientation distribution. Therefore, in tapes drawn at 120 °C, the crystals are less aligned in the drawing direction as compared to the tapes drawn at 80 °C. Next to this, the patterns show differences in the presence of homoepitaxially grown crystals indicated by (110) reflections in the meridional direction. These reflections are hardly visible in the diffraction pattern for 80 °C drawing temperature, while they are clearly observable for the tape drawn at 120 °C.

Figure 5 shows plots of one-dimensional intensity distributions as a result of an integration of 2-dimensional X-ray images along the azimuthal angle. Compared to the pattern of the as-extruded and drawn at 120 °C tapes, the (110) peak and the (040) peak shift closer together with decreasing postdrawing temperature. The (110) peak maximum shifts from $2\theta = 6.54°$ for the as-extruded tape to $2\theta = 6.71°$ for the tape postdrawn at 80 °C. For the tape drawn at 80 °C it is difficult to determine the precise 2θ value for the (040) peak maximum. Nevertheless, with decreasing drawing temperature a slight shift of the (040) peak toward lower angles can be observed. The peak shifts are not necessarily related to a change of the corresponding d values. The peak shifts may also result from a superposition of broad and overlapping (110) and (040) reflections.

Results of density measurements are shown in Figure 6. It can be seen that the density increases almost linearly with increasing drawing temperature, at least in the range from 80 to 120 °C. The calculated crystallinity increases from about 46.5% at 80 °C drawing temperature to 52.9% at 120 °C drawing temperature. The calculated mass crystallinity indices are not absolute values because the oriented amorphous phase in postdrawn tapes can have a slightly higher density than in the isotropic state. Therefore, the results display only a tendency.

Combining density and X-ray measurements, one can see that a variation in drawing temperature is related to a significant change in crystallinity, crystal size, and/or crystal perfection and orientation of these crystals.

To observe the changes in the amorphous region depending on the drawing temperature, retractive force experiments were performed. Upon heating, the material has the tendency to shrink. The hindered shrinkage (the tape is kept constrained within the clamps) results

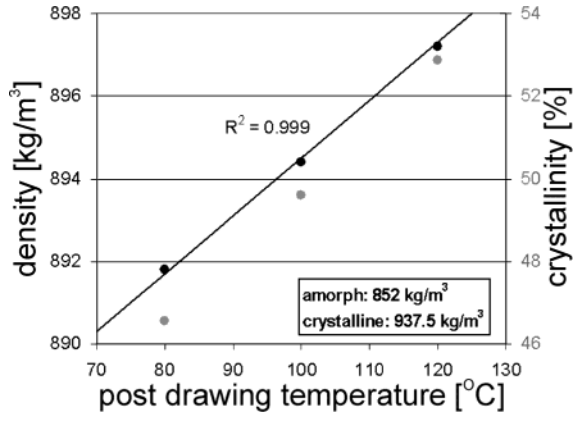

Figure 6. Density of the solid-state drawn iPP tapes in dependence to the drawing temperature. Indicated is also the calculated crystallinity using the two-phase model.

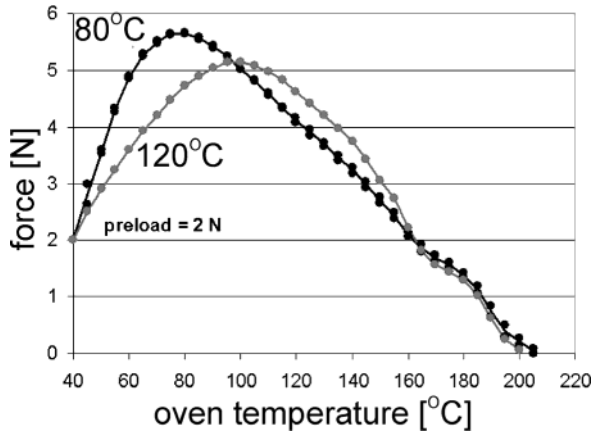

Figure 7. Retractive force measurements of solid-state drawn iPP tapes vs oven temperature.

in a force on the clamps, which is plotted against oven temperature in Figure 7. In the first part of the curve, the force increases due to the increasing effort of the amorphous phase to relax, the slope reflecting the initial degree of orientation within the amorphous region. At a certain temperature the force reaches a maximum, which corresponds to the onset of plastic deformation for the crystals. This deformation of the crystals results in a loosening of the molecules in the amorphous phase and hence in a reduction of the measured force. From distinct initial slopes and different temperatures of maximum forces it can be concluded that the organization of the amorphous phase varies significantly with changing the drawing temperature.

Discussion

The density, retractive force, and wide-angle X-ray measurements reveal that the drawing temperature has an enormous influence on internal structures and morphologies developed while solid-state postdrawing of iPP. Since mechanical properties depend on these features, iPP tapes and fibers show large differences in overall tensile behavior depending on the drawing temperature. While the measured stiffness is uniquely determined by the draw ratio, yield stress and elongation at break are strongly influenced by the applied drawing temperature.

A simplified model can explain the constant stiffness. According to Smith−Irvine, the stiffness depends on the applied network draw ratio. On the other hand, the network draw ratio determines the average orientation $\langle\cos^2\theta\rangle$ of statistical chain segments with respect to the drawing direction:

$$\langle\cos^2\theta\rangle = \frac{{\lambda_{net}}^3}{{\lambda_{net}}^3 - 1} - \frac{{\lambda_{net}}^3}{\sqrt{({\lambda_{net}}^3 - 1)^3}} \arctan\sqrt{({\lambda_{net}}^3 - 1)} \quad (7)$$

Therefore, the stiffness is related to the average chain segment orientation within the sample. The average chain segment orientation can be determined for example by birefringence measurements:

$$\Delta n = \Delta n_{max} \frac{3\langle\cos^2\theta\rangle - 1}{2} \quad (8)$$

In eq 8, Δn is the birefringence, while Δn_{max} is the birefringence of a perfectly oriented sample. The average chain segment orientation itself is composed of the chain segment orientation in the crystalline phase and the chain segment orientation in the amorphous phase under consideration of their composition:[6]

$$\Delta n = \Delta n_{cryst} X_c f_c + \Delta n_{amorph}(1 - X_c) f_a + \Delta n_{form} \quad (9)$$

where Δn_{cryst} and Δn_{amorph} are the intrinsic birefringence, and f_c and f_a are the Herman's orientation factors of the crystalline and amorphous regions, respectively; Δn_{form} is the so-called "form birefringence", taking in account the arrangement of crystalline and amorphous regions.

Therefore, different microscopic morphologies may result in the same averaged orientation, if the composition of crystalline and amorphous phase fulfills the equation above. The described "recipe" (eq 9) can explain the constant Young's modulus, although the amount and significance of each "ingredient" differs with drawing temperature. The authors are aware of the incompleteness of this explanation because interfaces of and interaction between crystalline and amorphous phase are not taken into account.

The dependence of yield stress on the postdrawing temperature may result from a transformation of monoclinic α-phase into a laterally disordered phase while postdrawing. For low temperatures the mobility of the molecules is very low because the drawing temperature is below the α-relaxation temperature of iPP. For this condition the formation of the disordered crystal structure would be preferred. This so-called mesomorphic phase has an ordered chain conformation, but a disordered lateral arrangement of left- and right-handed helices, which is less dense than an α-crystals.[23,24] The coherent interaction between the chains is weaker compared to the interaction within the α-phase. Therefore, shear forces required to deform the lateral disordered mesomorphic phase are lower than the shear forces required to deform the monoclinic α-phase. Consequently, the formation of mesomorphic phase leads to a decrease in yield stress. Studying melt-spinning of polypropylene, Sheehan and Cole found that the monoclinic α-phase has been formed under air-cooling conditions, while the mesomorphic phase has been induced by quenching in cold water.[5] Also, Nadella et al. could produce filaments containing this laterally disordered

phase by quenching the spun polymer into a water bath.[6] As reported by Fichera and Zannetti, the mesomorphic phase induced by quenching transforms to the stable monoclinic α-phase at temperatures above 70 °C.[25,26]

Porter et al. have mentioned for uniaxial compressed iPP that the mesomorphic phase can be also induced by solid-state deformation at proper processing conditions.[27] Depending on the deformation ratio, two different mechanisms are mentioned to form the mesomorphic phase: (1) "melting" of lamella fragments due to surface forces (for low deformation ratios) and (2) recrystallization of chains pulled out of lamella (for higher deformation ratios). In any case, the deformation temperature must be below a critical temperature $T_{critical}$, which depends on the applied deformation rate and hence on the hydrostatic pressure. In their studies of uniaxial compression, Porter et al. found $T_{critical}$ to be of the order of 120 °C. Therefore, deformation can induce the mesomorphic phase well above the stability limit for nondeformed, quenched samples. Possibly, the spin-line stress in the solid-state drawing stage influences the formation and stabilization of the mesomorphic phase in the same way as the hydrostatic pressure in the uniaxial compression.

Besides, it may be possible to induce the mesomorphic phase at oven temperatures above the 70 °C mentioned in the literature, even if the spin-line stress does not increase the stability limit. Because of its small thickness (±280 μm), the as-extruded tape seizes the oven temperature immediately. On the other hand, after leaving the oven, the even thinner postdrawn tape (±120 μm) cools to the ambient temperature also quite rapidly. Therefore, the laterally disordered phase can be obtained even at oven temperatures above 70 °C, if the residence time in the oven after deformation is shorter than the transition time from mesomorphic to α-crystal phase. The one-dimensional intensity scans of the wide-angle X-ray diffraction patterns (Figure 5) support the assumption of the formation of mesomorphic phase. As reported by Porter et al., the (110) and the (040) peak shift closer together if the mesomorphic phase is induced.[23] To verify this explanation of the drawing temperature dependence of the yield stress, further investigations are in progress, e.g., time-dependent density measurements at elevated temperature. Because of difference in density, the transition from mesomorphic to α-crystal phase should be displayed in the density vs time plot.

Conclusions

The effect of the temperature used on the mechanical properties as well as on the structure and morphology of solid-state drawn isotactic polypropylene has been described. It could be shown that the stiffness of the samples depends only on the applied draw ratio, which is in accordance with the Smith−Irvine model for an affine deformation. The average orientation of statistical chain segments ($\langle\cos^2\theta\rangle$) within the sample is independent of the drawing temperature. In contrast, yield stress and elongation at break are strongly influenced by the applied drawing temperature. For a fixed draw ratio, a significant drop in yield stress can be observed with lowering the drawing temperature. At a certain temperature this drop leads to a transition from brittle to ductile failure behavior, resulting in an increase of elongation at break. These differences in mechanical behavior can be explained by drawing temperature-dependent variations of the samples crystal structures and morphologies, which is displayed by differences in density, crystallinity, crystal size, and orientation of the crystal and amorphous phase. The main feature in this respect is the formation of the mesomorphic phase at low drawing temperatures. A possible explanation for this characteristic might be that the mobility of the molecules during deformation is very low because the drawing temperature is below the α-relaxation temperature of iPP. For this condition the formation of the disordered mesomorphic crystal structure would be preferred.

In conclusion, by choosing appropriate drawing conditions, the final mechanical properties can be tuned; to a certain extent stiffness, strength, and impact resistance can be tailored independently. Further investigations will be performed in order to confirm the formation of the mesomorphic phase at low drawing temperatures.

Acknowledgment. The authors are thankful to the R&D team from Lankhorst/Indutech B.V. for their help during tape manufacturing. We acknowledge Novem for financial support of the PURE project, within which the current studies were performed. The authors also thank Frank van de Burgt and Marco Hendrix for their support for X-ray investigation. Special thanks is extended to Cees Bastiaansen and Rudy Deblieck for their indefatigable readiness for discussions.

References and Notes

(1) Peijs, T. *Mater. Today* **2003**, *6*, 30.
(2) Loos, J.; Schimanski, T.; Hofman, J.; Peijs, T.; Lemstra, P. J. *Polymer* **2001**, *42*, 3827.
(3) Hoshino, S.; Powers, J.; Legrand, D. G.; Kawai, H.; Stein, R. S. *J. Polym. Sci.* **1962**, *58*, 185.
(4) Compostella, V.; Coen, A.; Bertinotti, F. *Angew. Chem.* **1962**, *74*, 618.
(5) Sheehan, W. C.; Cole, T. B. *J. Appl. Polym. Sci.* **1964**, *8*, 2359.
(6) Nadella, H. P.; Henson, H. M.; Spruiell, J. E.; White, J. L. *J. Appl. Polym. Sci.* **1977**, *21*, 3003.
(7) Spruiell, J. E.; White, J. L. *Polym. Eng. Sci.* **1975**, *15*, 660.
(8) Katayama, K.; Amano, T.; Nakamura, K. *Kolloid Z. Z. Polym.* **1968**, *226*, 1250.
(9) Kitao, T.; Ohya, S.; Furukawa, J.; Yamashita, S. *J. Polym. Sci.* **1973**, *11*, 1091.
(10) Lu, F.; Spruiell, J. E. *J. Appl. Polym. Sci.* **1987**, *34*, 1521.
(11) Lu, F.; Spruiell, J. E. *J. Appl. Polym. Sci.* **1987**, *34*, 1541.
(12) Bodaghi, H.; Spruiell, J. E.; White, J. L. *Int. Polym. Process.* **1988**, *3*, 100.
(13) Hahn, K.; Kerth, J.; Zolk, R.; Schwahn, D.; Springer, T.; Kugler, J. *Macromolecules* **1988**, *21*, 1541.
(14) Diacik, I.; Durcova, O.; Diacik, I., Jr.; Mitterpachova, M. *Acta Polym.* **1988**, *39*, 391.
(15) Gill, R. A.; Benjamin, C. *Plast. Rubbers: Process.* **1980**, *5*, 25.
(16) Andreassen, E.; Myhre, O. J.; Hinrichsen, E. L.; Gråstad, K. *J. Appl. Polym. Sci.* **1994**, *52*, 505.
(17) Irvine, P. A.; Smith, P. *Macromolecules* **1986**, *19*, 240.
(18) Kuhn, W.; Grün, F. *Kolloid Z. Z. Polym.* **1942**, *101*, 248.
(19) Tung, L. H.; Taylor, W. C. *J. Polym. Sci.* **1956**, *21*, 144.
(20) Kilian, H. G. *Kolloid Z. Z. Polym.* **1961**, *176*, 49.
(21) Nurul Huda, M.; Dragaun, H.; Bauer, S.; Muschik, H.; Skalicky, P. *Colloid Polym. Sci.* **1985**, *263*, 730.
(22) Dirix, Y. J. L. Ph.D. Thesis, ISBN 90-386-0868-3, 1997; Chapter 2, p 24.
(23) Brückner, S.; Meille, S. V.; Petraccone, V.; Pirozzi, B. *Prog. Polym. Sci.* **1997**, *16*, 361.
(24) Auriemma, F.; de Ballesteros, O. R.; de Rosa, C.; Corradini, P. *Macromolecules* **2000**, *33*, 8764.
(25) Fichera, A.; Zannetti, R. *Makromol. Chem.* **1975**, *176*, 1885.
(26) Zannetti, R.; Celotti, G.; Fichera, A.; Francesconi, R. *Makromol. Chem.* **1969**, *128*, 137.
(27) Saraf, R. F.; Porter, R. S. *Polym. Eng. Sci.* **1988**, *28*, 842.

MA034949S